JOURNAL OF MATERIALS SCIENCE 26 (1991) 4313–4317

Microstructure and physical properties of transparent thoria–yttria ceramics

M. HARTMANOVÁ, V. ŠÁLY
Institute of Physics, Slovak Academy of Sciences, Bratislava, Czechoslovakia
F. HANIC, M. PISARČÍK
Institute of Inorganic Chemistry, Slovak Academy of Sciences, Bratislava, Czechoslovakia
H. ULLMANN
Central Institute for Nuclear Research, Academy of Science, 8051 Dresden, FRG

The investigation of microstructure, some electrical and optical parameters of transparent ThO_2–15 mol % $YO_{1.5}$ ceramics has shown: (a) a very low porosity, close to zero; (b) a higher electrical conductivity than is usual for ThO_2 ceramics of the same composition, with the activation energy 1.12 eV; (c) a relative permittivity $\varepsilon_r \sim 33$ under the given conditions; (d) confirmation of a single-phase fluorite-type cubic structure by means of Raman and infrared spectra.

1. Introduction

Among the solid oxide electrolytes, zirconia and thoria base materials are the most important for applications in high-temperature galvanic cells, fuel cells, oxygen gauges and oxygen pumps. These materials are predominantly oxygen ion conductors over a wide range of temperature and oxygen partial pressure. Compared with zirconia-base electrolytes, thoria-base materials show one or two orders of magnitude lower electrical conductivity and are useful at the lower oxygen partial pressure range. At higher oxygen partial pressures, the conductivity is predominantly of p-type [1–3].

Thorium dioxide, ThO_2, has the cubic CaF_2-type structure up to its melting point, 3300 °C. Under the special technological conditions, it is possible to prepare transparent ThO_2–$YO_{1.5}$ ceramics (e.g. [4]) practically with the theoretical density.

The aim of the present work was to describe the structural modification and microstructure of investigated system from different points of view and to investigate some electrical parameters.

2. Experimental procedure

2.1. Preparation

The transparent ceramics have been obtained by the oxalate method to produce homogeneous powder compositions containing ThO_2 and Y_2O_3 and by the sintering at 1850 °C for 5 h in flowing hydrogen to obtain the maximum density [5].

2.2. Density

The observed density was determined using a previously calibrated pycnometer. Distilled water was used as a liquid medium. The air bubbles were removed by reducing the pressure. An accuracy of better than 0.05% has been achieved with this technique.

2.3. Unit cell parameter, *a*

The unit cell parameter, *a*, of the cubic $Y_{0.15}Th_{0.85}O_{1.925}$ phase was determined by X-ray powder diffractometry using a Philips 1540 diffractometer and CuK_α radiation. The parameter, *a*, was evaluated from the line separation $\Delta\theta = \theta_i - \theta_j$ of the corresponding α_1 or α_2 components of the Bragg reflection doublets of the *i*th and *j*th lines. The Bragg angles were measured up to $2\theta \leqslant 140°$.

2.4. Microstructure

The grain boundaries in dense polycrystalline samples were revealed by the gradual etching of the samples in pure H_3PO_4 acid at 168–190 °C over 6 min. The microstructure of the etched surfaces was observed under SEM Tesla BS 300 at the accelerated voltage of 25 kV.

2.5. Electrical parameters

These have been investigated in the frequency range from 10–10^5 Hz at temperatures 300–427 °C in air. The conductance and capacitance were measured by means of a GR Capacitance bridge 1616. The temperature was stabilized by a Chinoterm 10 A digital temperature controller with an accuracy of $\pm$ 0.5 °C. The influence of the annealing temperature on the measured and calculated parameters of samples was negligible.

0022–2461/91 $03.00 + .12

2.6. Optical properties

Raman and infrared spectra have been investigated. Raman spectra were measured on a Laser Raman Spectrometer JRS-S1 Jeol using the green line (514.5 nm) of an argon-ion laser. The excited energy of the laser beam was 100 mW.

The infrared spectra (4000–200 cm^{-1}) were measured on a double grating infrared spectrometer (Perkin–Elmer 983 G). No infrared and Raman polarization studies were made. All measurements were performed at room temperature.

3. Results and discussion

3.1. Density and microstructure

The porosity of the sample was tested by comparison of the calculated and measured density. The calculated value, D_c, was obtained from the relation

$$D_c = \frac{Z\,\mathrm{MW}\,A}{V} \tag{1}$$

where Z is the number of formula units, $Y_{0.15}Th_{0.85}O_{1.925}$, in the unit cell ($Z = 4$), MW is the molecular weight of the formula unit (241.44), A is the Avogadro number and V is the unit cell volume (173.77×10^{-30} m^3). The calculated density of $Y_{0.15}Th_{0.85}O_{1.925}$ is 9231 $kg\,m^{-3}$.

The measured density, $D_m = 9227(5)$ $kg\,m^{-3}$ (22 °C), compared with the calculated value, confirmed a very low porosity, close to zero.

The microstructure of the etched surface of the sintered sample is shown in Fig. 1. The average grain size, $\bar{D}$, was found to be 2.23 μm. This value is much smaller than the value obtained by Greskovich *et al.* [4] for the transparent sample of the same composition, where $\bar{D} \sim 140$ μm. The difference is caused by the higher sintering temperature (2380 °C) and longer sintering time (20 h) used in paper [4] in comparison with the conditions used here. The lattice parameters of systems of the same composition in [4] and in the present work, were found to be practically the same.

3.2. Electrical parameters

The ThO_2–$YO_{1.5}$ ceramic is a mixed, ionic–electronic conductor. The ionic charge carrier in this system is the oxygen ion vacancy (e.g. [1–3, 6, 7]) which is represented by the following reaction

$$(1 - x)\,ThO_2 + xYO_{1.5} \rightarrow Th_{1-x}Y_xO_{2-x/2} + x/2V_O^{\cdot\cdot} \tag{2}$$

where x is the number of Y^{3+} ions substitutionally incorporated instead of Th^{4+} in the lattice. A higher value of x means a higher concentration of oxygen ion vacancies and thus a higher conductivity. However, when the concentration of oxygen ion vacancies is sufficiently high to cause lattice distortion, defect interactions or vacancy clustering and ordering, their statistical distribution loses its disordered state and it transforms to an ordered one restricting the ionic conductivity. The ionic conductivity can be expressed (Kröger–Vink notation) as

$$\sigma_{ion} = [V_O^{\cdot\cdot}]\,2e\mu \tag{3}$$

where e is electronic charge and μ is ionic mobility. The p-type conductivity at higher oxygen pressures (e.g. the measurement performed in air) results from a

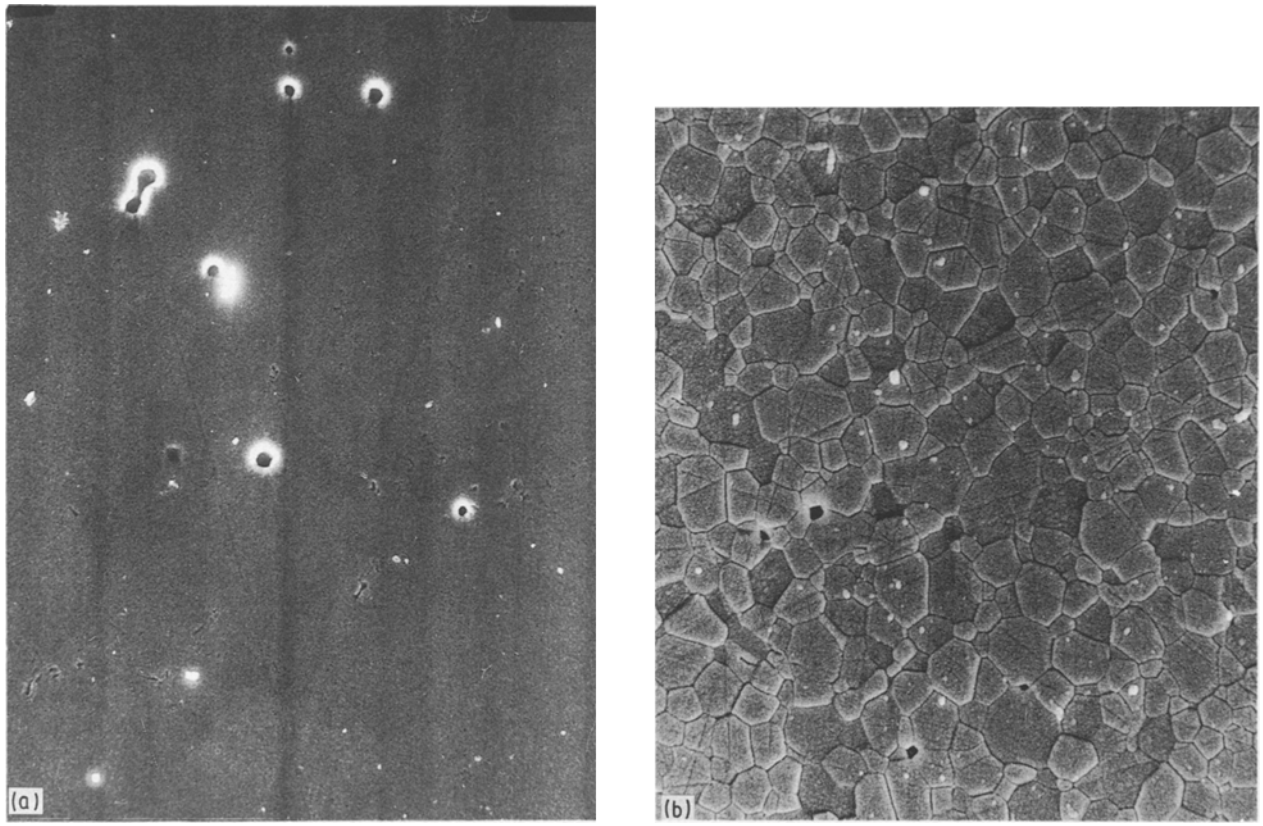

Figure 1 The microstructure of ThO_2–15 mol % $YO_{1.5}$ (a) without etching, (b) chemically etched. ×4000.

dissolution of oxygen into the lattice according to

$$1/2\ O_2(g) + V_O^{\cdot\cdot} \rightarrow O_O + 2\,h^{\cdot}$$

$$\sigma_p \sim P_{O_2}^{1/4} \qquad (4)$$

where O_O is an oxygen ion on a normal lattice site and $h^{\cdot}$ is an electron hole. P_{O_2} is the oxygen partial pressure.

The electrical parameters were investigated by means of impedance spectroscopy and analysed in the complex plane. The frequency dependence of complex impedance at two temperatures is shown in Fig. 2. The dependence has the characteristic shape of a semicircle with the centre under the real axis at high frequencies and low temperatures. The influence of the electrode/electrolyte interface appears on the low-frequency part of the diagram with an increase in the temperature. The shape of this part of diagram is dependent on the electrode areas of the measured cell O_2, Pt|ThO_2–$YO_{1.5}$|Pt, O_2.

The frequency dependence of the complex permittivity components of sample can be seen in Fig. 3. The relative permittivity, ε_r, of ThO_2 doped with $YO_{1.5}$ (prepared according to the noted technology) at temperature $T = 300\,^{\circ}C$ and frequency $f \sim 10^5$ Hz was found to be ~ 33.

The frequency dependences of measured values of capacitance, C_p, and conductance, G_p, are shown in Fig. 4. The dependences of $\log C_p = f(\log f)$ and $\log(G_p - 1/R_p) = f(\log f)$ are linear at high frequencies and low temperatures, where R_p is the resistance. Thus [8]

$$C_p \sim B_B\,\omega^{-\delta} \qquad (5)$$

and

$$G_p \sim A_B\,\omega^{\beta} \qquad (6)$$

where $\log B_B (\log A_B)$ is a point of intersection of the straight line dependence with the vertical axis and the exponent $\delta(\beta)$ is a straight line slope.

The R_B value is obtained from the complex impedance diagram in Fig. 2. $1/R_B(d/S)$ is assumed to be the grain bulk conductivity of solid electrolyte ThO_2–Y_2O_3 [8]. The temperature dependence of the total electrical conductivity has an Arrhenius character in the investigated temperature range

$$\sigma T = A \exp(-E_A/kT)$$

where σ is the conductivity, A is the pre-exponential factor, E_A is the activation energy and kT is the Boltzmann factor. The activation energy of bulk conductivity, E_A, was found to be -1.12 eV (Fig. 5).

The samples prepared by means of the noted technology have a higher conductivity than is usual for ThO_2 ceramics doped with Y_2O_3 (see e.g. [6, 9]).

3.3. Optical properties

The X-ray measurements of transparent ThO_2–15 mol % $YO_{1.5}$ demonstrated the existence of a single-phase structure of the fluorite type [5]. The Raman and infrared reflectivity spectra at room temperature have been used to describe the structural modification from other points of view.

The crystal structure of $YO_{1.5}$-doped thoria is a disordered fluorite type. Th^{4+} ions are partly replaced by Y^{3+} ions at random. This means that some oxygen sites remain vacant, keeping charge neutrality. Therefore, the cubic thoria loses the translation symmetry

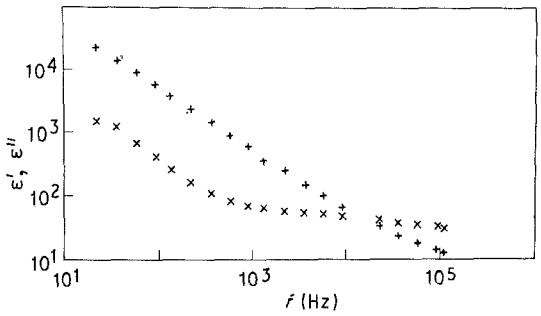

Figure 3 The frequency dependence of complex permittivity of ThO_2–15 mol % $YO_{1.5}$. (×) ε', (+) ε'', $\theta = 301\,^{\circ}C$.

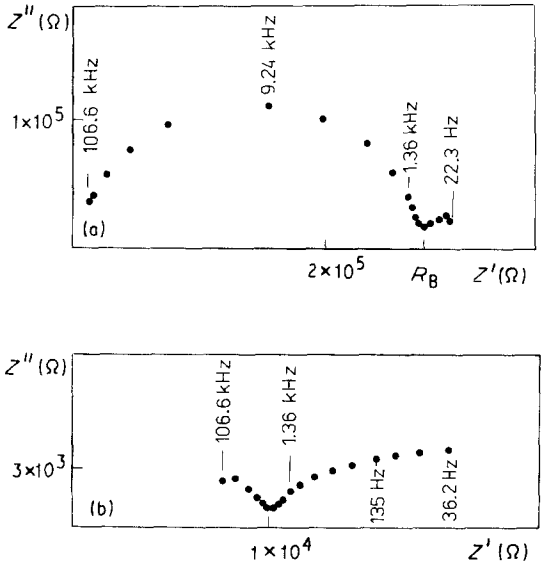

Figure 2 The complex impedance diagram of ThO_2–15 mol % $YO_{1.5}$ at (a) 301 °C, and (b) 397 °C.

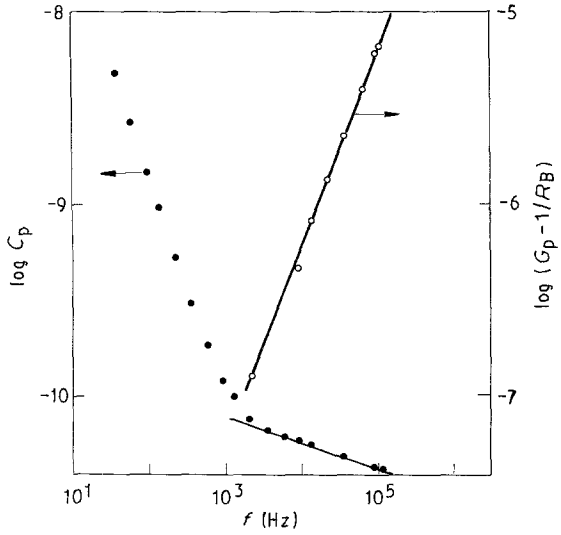

Figure 4 The capacitance and conductance of cell O_2, Pt|ThO_2–$YO_{1.5}$|Pt, O_2.

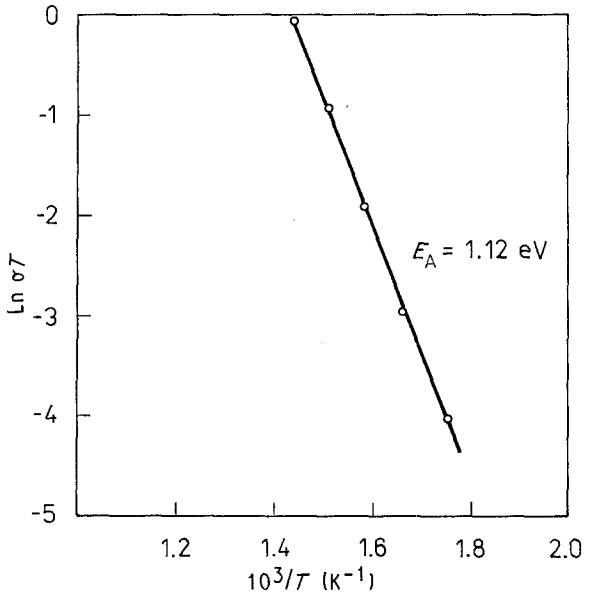

Figure 5 The temperature dependence of total electrical conductivity of ThO_2–15 mol % $YO_{1.5}$.

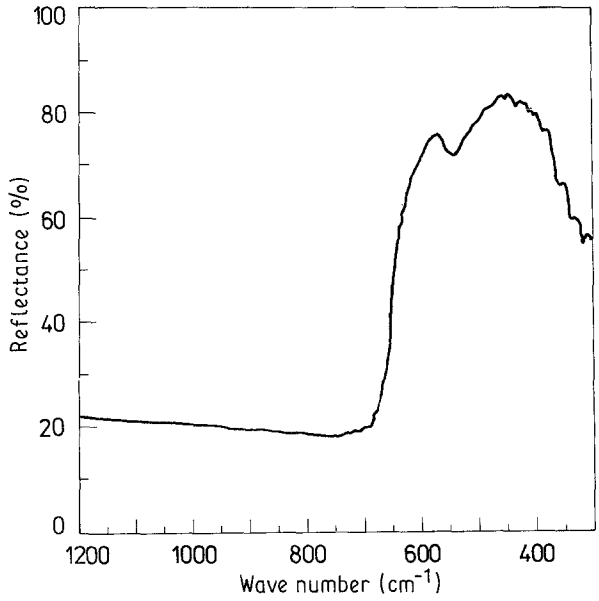

Figure 7 The infrared reflectance of ThO_2–15 mol % $YO_{1.5}$ observed at room temperature.

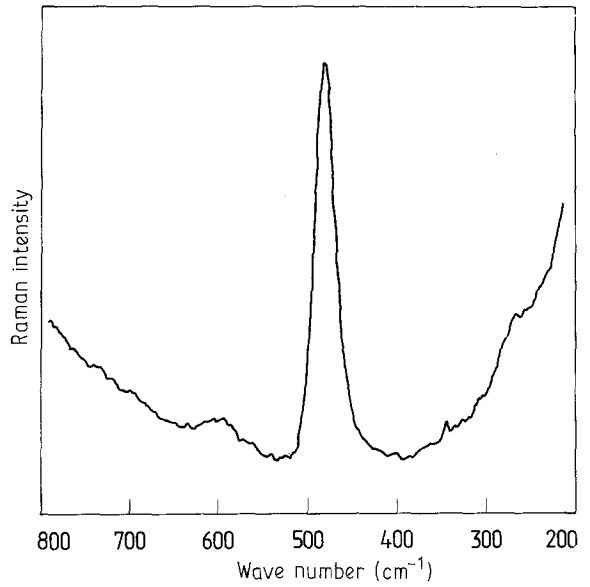

Figure 6 The Raman spectrum of ThO_2–15 mol % $YO_{1.5}$ observed at room temperature.

of the crystal. The loss of translation symmetry destroys the wave vector $k = 0$ selection rule for the Raman scattering and the infrared absorption in the crystal. Consequently, the phonons at all parts in the Brillouin zone will contribute to the optical spectra.

Generally, the cubic crystals with the fluorite structure and space group Fm3m (O_h^5) have an exceptionally simple vibrational structure with one infrared active phonon of T_{1u} symmetry and one Raman active phonon of T_{2g} symmetry at $k = 0$ [10]. However, for the cubic zirconia, for instance, the spectra with symmetries A_{1g} and E_g are also observed in addition to the spectra with symmetry T_{2g} [11]. Furthermore, each polarized spectrum exhibits many structures with large linewidths. In particular, a continuously spread band is observed for T_{2g} symmetry in contrast with the T_{2g} band with the half width of about 7 cm^{-1} for ThO_2 crystal [10, 12].

The obtained results are shown in Fig. 6. Only a single sharp line corresponding to the T_{2g} mode was observed in the Raman spectrum under the stated conditions. Such a mode between 400 and 500 cm^{-1} is observed in CeO_2 at 465 cm^{-1}, UO_2 at 467 cm^{-1} and ThO_2 at 466 cm^{-1} in [10]. In this mode, two neighbouring substitutional oxygen ions move in opposite directions. The total dipole moment of this excitation is 0, as expected for the Raman-active mode. Depending upon the type of solid solution, in some cases, apart from the intrinsic T_{2g} phonon, additional Raman modes can be observed [13].

The symmetry arguments support the experimental observation of a single, strong infrared resonance in the investigated structure (Fig. 7). The spectrum obtained is in good agreement with [14].

4. Conclusion

The Raman and the infrared spectra confirmed the single-phase cubic structure of the fluorite type with a very low porosity close to zero. The electrical conductivity was found to be higher than is usual for ceramics of the same composition, but not transparent.

Acknowledgement

The authors thank Dr E. Morháčová for the determination of average grain size.

References

1. J. M. WIMMER, L. R. BIDWELL and N. M. TALLAN, *J. Amer. Ceram. Soc.* **50** (1967) 198.
2. E. C. SUBBARAO, P. H. SUTTER and J. HRIZO, *ibid.* **48** (1965) 443.
3. T. H. ETSELL and S. N. FLENGAS, *Chem. Rev.* **70** (1970) 339.

4. C. GRESKOVICH, C. R. O'CLAIR and M. J. CURRAN, *J. Amer. Ceram. Soc.* **55** (1972) 324.
5. T. REETZ, I. HAASE, H. ULLMANN, H.-J. LANG, F. HANIC, V. ŠÁLY and M. HARTMANOVÁ, *Solid State Ionics* **36** (1989) 193.
6. M. HARTMANOVÁ, F. HANIC, A. KOLLER and J. JANČI, *Czech. J. Phys.* **B28** (1978) 414.
7. M. HARTMANOVÁ, *Acta Phys. Slov.* **28** (1978) 188.
8. I. D. RAISTRICK, CHUN HO, and R. A. HUGGINS, *J. Electrochem. Soc.* **123** (1976) 1469.
9. H. NÄFE, *Solid State Ionics* **13** (1984) 255.
10. V. G. KERAMIDAS and W. B. WHITE, *J. Chem. Phys.* **59** (1973) 1561.
11. M. ISHIGAME and M. KOJIMA, *Solid State Ionics*, **23** (1987) 211.
12. *Idem, J. Phys. Soc. Jpn* **41** (1976) 202.
13. D. J. OOSTRA and H. W. DEN HARTOG, *Phys. Rev.* **B29** (1984) 2423.
14. J. D. AXE and G. D. PETTIT, *Phys. Rev.* **151** (1966) 676.

Received 19 January
and accepted 29 October 1990